JOURNAL OF THERMOPHYSICS AND HEAT TRANSFER
Vol. 21, No. 3, July–September 2007

Transient Modeling of Loop Heat Pipes for the Oscillating Behavior Study

Stéphane Launay,* Vincent Platel,† Sébastien Dutour,‡ and Jean-Louis Joly§
Université Paul Sabatier, 31062 Toulouse Cedex, France

DOI: 10.2514/1.26854

A transient overall model has been developed to predict the thermal and hydrodynamic behavior of a standard loop heat pipe. The model of the loop has been divided into subsystems, for which transient mass, energy, or momentum conservation laws have been developed. The comparison of the calculation and experimental results for a transient test allows one to validate the proposed model. Then, the model is used to study the development mechanisms of an oscillating behavior during the loop heat pipe operation. Two different patterns of temperature fluctuation have been highlighted by modifying the loop heat pipe external conditions (heat load, sink temperature, ambient heat exchange with the liquid line). The characteristics of these oscillations are then compared quantitatively to available experimental tests: these comparisons highlight the ability of the model to accurately predict the frequencies and amplitudes as well as how they are affected by the design and operational parameters.

Nomenclature

A	=	cross-sectional area, m^2
c_p	=	specific heat capacity at constant pressure, $J \cdot kg^{-1} \cdot K^{-1}$
D	=	diameter, m
dw	=	element volume, m^3
g	=	gravity, $m \cdot s^{-2}$
h	=	enthalpy, $J \cdot kg^{-1}$ or heat transfer coefficient, $W \cdot m^{-2} \cdot K^{-1}$
L	=	length, m
ℓ_v	=	heat of vaporization, $J \cdot kg^{-1}$
$\dot{m}$	=	mass flow rate, $kg \cdot s^{-1}$
$\dot{m}^*$	=	vaporized mass flow rate, $kg \cdot s^{-1}$
p	=	pressure, Pa
$\dot{Q}_{\text{load}}$	=	heat load, W
$\dot{Q}_p$	=	parasitic heat flux, W
R	=	thermal resistance, $K \cdot W^{-1}$
r	=	gas constant, $J \cdot kg^{-1} \cdot K^{-1}$
S	=	liquid surface area, m^2
T	=	temperature, K or °C
t	=	time, s
$\bar{\alpha}$	=	vapor fraction in the two-phase flow region of the condenser
$\bar{\eta}$	=	two-phase zone length in the condenser, m
θ	=	inclination angle from vertical, rad
μ	=	dynamic viscosity, $kg \cdot s^{-1} \cdot m^{-1}$
ρ	=	density, $kg \cdot m^{-3}$
ϕ	=	heat rate, W
Ω	=	volume, m^3

Subscripts

amb	=	ambient
ax	=	axial
C	=	condenser
conv	=	convection
E	=	evaporator
exp	=	experimental
i	=	inlet
L	=	liquid line
ℓ	=	liquid
m	=	metal
o	=	outlet
R	=	reservoir
rad	=	radiator
sub	=	subcooled region
V	=	vapor line
v	=	vapor
vap	=	vaporization surface
w	=	wick
2φ	=	two-phase mixture

Received 1 August 2006; revision received 26 January 2007; accepted for publication 9 February 2007.

*Ph.D. Researcher, Laboratoire d'Energétique.
†Assistant Professor, Laboratoire d'Energétique (Corresponding Author).
‡Assistant Professor, Laboratoire d'Energétique.
§Professor, Laboratoire d'Energétique.

I. Introduction

IN THE field of electronic industry, the component development aims at the performance increase and the miniaturization of electronic devices both resulting in an increase of the heat flux dissipation. To insure a high component reliability, which is closely dependent on the component temperature level, the thermal management in electronics becomes a major challenge. As conduction or air convection cooling systems are no longer efficient to transfer such high heat fluxes, alternative cooling techniques have to be developed. Because of the efficiency of vaporization and condensation heat transfer and the flexibility of the fluid transport processes, passive two-phase closed systems are very attractive for transferring large heat fluxes with small temperature differences.

Among them, the loop heat pipe (LHP) is a specific capillary-driven two-phase heat transport device, whose operating principle was presented by Ku [1]. Figure 1 shows the schematic of a simplified LHP. A LHP consists of an evaporator, a condenser, a compensation chamber (also called reservoir), and vapor and liquid transport lines. The capillary forces, which are developed at the liquid/vapor menisci in the porous wick of the evaporator, induce the fluid displacement along the loop, transferring the heat from the evaporator to the condenser sections. Compared to conventional heat pipes, LHPs possess some additional advantages in the framework of the capillary mechanism. This includes a maximum decrease in the distance of the liquid motion in the wick (limited to the evaporator section), which induces a maximum decrease of the pressure drop all along the loop for an identical mass flow rate. This property enables the use of wicks of very small pore diameters to increase the "maximum" capillary pumping limit. Thus, the heat can be transferred up to several meters at any orientation in the gravity field.

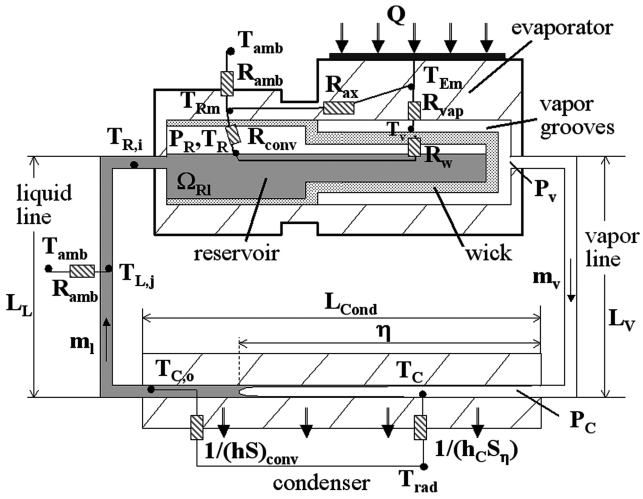

Fig. 1 Schematic of a loop heat pipe.

Compared to the capillary pumped loop (CPL), which has the same basic operating principle, the LHP two-phase reservoir is directly connected to the evaporator by the use of a secondary wick (Nikitkin and Cullimore [2]). This physical proximity of the reservoir to the evaporator simplifies the LHP startup and avoids the loop failure when some vapor amount enters the evaporator core. Both contribute to the robustness of the LHP operation under various conditions. Consequently, the LHP original conception allows a wide variety of different design embodiments, as the flexibility in evaporator/condenser locations, which essentially extends the sphere of functional possibilities and practical applications of these devices (Maydanik [3]).

Despite the design simplicity and the theoretical operational robustness, various nondesirable LHP behaviors have been experimentally observed consequently to transient changes, such as the startup or variations in the heat load and/or the sink temperature (Kaya and Ku [4]). Sometimes, the LHP never really reaches a steady-state temperature but instead displays an oscillating behavior (Ku [5], Ku and Rodriguez [6], Chen et al. [7]). Three types of temperature oscillation regimes have been reported in the literature by Ku [5] and Ku and Rodriguez [6]: 1) ultrahigh-frequency (period of about a second or less) temperature oscillations; 2) high-frequency (period of a few seconds or minutes) low-amplitude oscillations caused by the inability of the vapor front to find a stable position inside the condenser; 3) low-frequency (period of about hours) high-amplitude oscillations, which may appear for specific conditions as, for example, large evaporator thermal inertia, low heat load, and cold sink temperature compared to the ambient one. As type 1 is usually assumed to be induced because of the liquid slug formation in the condenser or in the vapor line, types 2 and 3 are typically induced by the original complex couplings of the thermal and hydrodynamic mechanisms involved by the interactions between the loop components. The amplitude of the temperature variations at the evaporator saddle can reach 1–10 K. Such versatile dynamic behaviors are not suitable and have to be avoided. Thus, to understand and control such oscillating behaviors, it is essential to develop, in parallel with the physical analysis provided by the experiments, a transient model able to describe the complexity of the LHP dynamic at the whole system level.

Various models have been developed for the LHP characterization but essentially at steady state because of their use to dimension new-designed LHP (Kaya and Hoang [8], Furukawa [9]). Concerning the development of the LHP transient modeling, only a limited amount of publications exist in the open literature. Mena et al. [10] have developed a transient model based on the energy and mass balance equations in a monodimensional hydraulic network. The mass flow rate was assumed to be constant at each instant in the whole loop and the pressure energy was neglected. By comparing the calculation and experimental results, Mena et al. [10] concluded that this modeling approach did not allow one to perform very accurate thermohydraulic analysis at the LHP level during the transient changes. Wrenn et al. [11] have used the NASA-standard thermohydraulic analyzer, SINDA/FLUINT, which solves the conservation equations of mass, momentum, and energy. The LHP transient model was not clearly detailed. The calculation results, presented by Wrenn et al. [11], showed good agreement with the experimental LHP dynamic behavior, which is generated by transient changes in the LHP boundary conditions. The combined transient model, developed by Vlassov and Riehl [12], consists of a detailed model of the condenser and a coarse model of the evaporator/reservoir. From the mass, momentum, and energy conservation equations, only mass and thermal inertia terms have been considered. Comparing the model and experimental results, the LHP dynamic behavior has been correctly predicted within 3–4 K of accuracy, by adjusting several evaporator parameters. Although these different models seem to correctly simulate the LHP dynamic behavior, none of them present any results on the model capability to determine any types of oscillations.

The transient overall LHP model presented in this study has been developed to predict such LHP dynamic behaviors and to characterize the LHP oscillations, such as the frequency and the amplitude, during all operational conditions and in relation with the geometrical and physical parameters of the loop. The originality of the proposed modeling approach consists of simplifying the most geometrically or technologically complex elements while assuming that the global distribution of the fluid phases and the displacement of the liquid–vapor interfaces are relevant to describe the fluid dynamics. The model is detailed in Sec. II. The LHP geometry and the experimental results, presented by Wrenn et al. [11], were sufficiently detailed that they could be used for the model validation. The model validation and the prediction of various LHP oscillating behaviors are presented in Sec. III.

II. Model Description

The transient modeling of the overall loop is divided into four subsystems, which are thermally and/or hydrodynamically interconnected. The subsystems are as follows: 1) the fluid in the compensation chamber, 2) the evaporator and the reservoir wall, 3) the fluid in the condenser, and 4) the fluid in the transport lines. The conservation laws and the assumptions will be presented for each subsystem. The fluid thermophysical properties vary with each subsystem temperature.

A. Compensation Chamber Subsystem

The compensation chamber subsystem is composed of the fluid (liquid and vapor) in the reservoir and in the evaporator core (do not include the capillary wick). The two-phase fluid in the compensation chamber subsystem is supposed to be at the saturation state. The liquid phase is considered incompressible and the vapor phase is assumed compressible. The fluid phase distribution between the reservoir and the evaporator core may have an effect on the LHP operation (Ku [1]). However, the fluid phase distribution is difficult to estimate as it strongly depends on the LHP orientation, the evaporator/reservoir design (without or with a bayonet), and the initial fluid charge. In the first approach, the effect of the fluid phase distribution on the LHP operation is neglected. The evaporator core is assumed to be filled with vapor, whatever the LHP operating conditions, which tends to overestimate the evaporator/reservoir heat leak during specific LHP operations.

The liquid charge variation in the compensation chamber is defined by the mass balance law between the fluid mass flow rate incoming from the liquid line $\dot{m}_\ell$, the liquid mass flow rate passing through the evaporator primary wick for evaporation $\dot{m}_v$, and the eventual evaporation–condensation mass flow rate at the liquid/vapor interface in the reservoir. By introducing the Clausius–Clapeyron equation and assuming that the vapor behaves as a perfect gas, the mass conservation equation in the reservoir leads to

$$(\rho_\ell - \rho_{v_R})\frac{\partial \Omega_{R_\ell}}{\partial t} + (\Omega_R - \Omega_{R_\ell})\left(\frac{\ell_v \rho_\ell \rho_{v_R}}{rT_R^2(\rho_\ell - \rho_{v_R})} - \frac{\rho_{v_R}}{T_R}\right)\frac{\partial T_R}{\partial t} = \dot{m}_\ell - \dot{m}_v \quad (1)$$

where Ω_{R_ℓ} is the volume occupied by the liquid in the reservoir.

The transient energy balance inside the compensation chamber establishes the reservoir temperature T_R during the transient changes of the reservoir input parameters. Balancing the energy will obtain

$$\frac{d}{\mathrm{d}t}\int_{\Omega_{R_\ell}} \rho_\ell h_\ell \,\mathrm{d}\omega + \frac{d}{\mathrm{d}t}\int_{\Omega_{R_v}} \rho_{v_R} h_v \,\mathrm{d}\omega - \frac{d}{\mathrm{d}t}\int_{\Omega_R} p_R \,\mathrm{d}\omega = \dot{m}_\ell h_\ell(T_{R,i}) - \dot{m}_v h_\ell(T_R) + \dot{Q}_p \quad (2)$$

where the left-hand terms of Eq. (2) characterize the reservoir liquid and vapor thermal inertia effects, and the right-hand terms correspond to the energy of the return subcooled liquid, the energy of the liquid removed by the wick for the evaporation, and the net thermal energy received by the compensation chamber. Using similar assumptions as for the mass balance, Eq. (2) becomes

$$\left\{[\rho_\ell \Omega_{R_\ell} + (\Omega_R - \Omega_{R_\ell})\rho_{v_R}]\left[c_{p_\ell} + \frac{\ell_{v_R}\rho_{v_R}}{T_R(\rho_\ell - \rho_{v_R})}\right] + (\Omega_R - \Omega_{R_\ell})\frac{\ell_{v_R}}{rT_R}\left[\frac{\ell_{v_R}\rho_\ell\rho_{v_R}}{T_R(\rho_\ell - \rho_{v_R})} - r\rho_{v_R}\right] - \Omega_R \frac{\ell_{v_R}\rho_\ell\rho_{v_R}}{T_R(\rho_\ell - \rho_{v_R})}\right\}\frac{\mathrm{d}T_R}{\mathrm{d}t} - \rho_{v_R}\ell_v\frac{\mathrm{d}\Omega_{R_\ell}}{\mathrm{d}t} = \dot{m}_\ell c_{p_\ell}(T_{R,i} - T_R) + \dot{Q}_p \quad (3)$$

The heat leak $\dot{Q}_p$, the liquid and vapor mass flow rates, $\dot{m}_\ell$ and $\dot{m}_v$, respectively, and the reservoir inlet liquid temperature $T_{R,i}$ correspond to the reservoir model input parameters. They are deduced from the other subsystems of the LHP. The time variations of the reservoir liquid volume Ω_{R_ℓ} and the reservoir temperature T_R are deduced from the differential equations (1) and (3). By considering the reservoir in a two-phase equilibrium state, the reservoir pressure p_R is a function of the reservoir saturation temperature T_R. Such a subsystem is a source of thermal and hydrodynamic couplings.

B. Evaporator Subsystem

The evaporator subsystem is composed of the evaporator and reservoir metal masses, the vapor grooves, and the capillary wicks. The heat transfer process involves metal thermal inertia, conduction of heat from the heat source $\dot{Q}_{\mathrm{load}}$ into the pump body, and evaporation of liquid at the primary wick outer surface. Vapor vented into the vapor grooves is carried away to the vapor line. No fluid accumulation into the evaporator subsystem has been considered, which means that the porous wick remains saturated with liquid and that the vapor grooves are filled with vapor. This last condition will not be appropriate for LHP previously to start up, for which the vapor grooves can be initially filled or partially filled with liquid. The vapor pressure drop in the evaporator is assumed to be small, such that the vapor can be considered isothermal. Considering the vapor grooves in a two-phase saturation state, the vapor temperature T_v is deduced from the vapor pressure p_v, which is calculated in the vapor line subsystem.

The evaporator subsystem heat transfer can be simplified to a thermal nodal network. The heat load distribution from the heat source to the evaporator area and to the compensation chamber is regulated by means of five thermal resistances, shown in Fig. 1. They are defined as 1) R_{vap}, the thermal resistance from the heat source to the evaporation interface at the porous wick surface. R_{vap} is a combination of heat conduction in the metal mass, heat conduction in the porous wick until the evaporation interface, and evaporation heat transfer. R_{vap} is difficult to characterize. On one hand, Zhao and Liao [13] experimentally showed that the evaporation heat transfer, which takes into account the liquid recession into the wick, varies as a function of the imposed heat flux. On the other hand, it is difficult to estimate the liquid front position into the porous wick as it may depend on the porous characteristics (Delil et al. [14]), the LHP orientation and tilt, the fluid/wick wettability, and the system conditions (gravity, temperature, heat flux, etc.). Consequently, R_{vap} is first considered as a constant in the proposed model, which means that the conduction resistance is dominant compared to the evaporation resistance for the studied heat load range. 2) R_{ax} is the axial conduction resistance between the evaporator and the compensation chamber metal body. 3) R_w is the overall thermal resistance through the porous wick. R_w may vary depending on the liquid/vapor distribution in the evaporator core and depending on the convection heat transfer compared to the conduction heat transfer in the porous wick. Using nondimensional numbers, a detailed analysis of the convection–conduction heat transfer in the porous wick has been presented by Mishkinis and Ochterbeck [15] for two wick effective thermal conductivities. Considering a high effective thermal conductivity of the porous wick and low flow rates, R_w may be considered as a constant conduction resistance. 4) R_{conv} is the convection resistance between the metal mass and the fluid of the compensation chamber, and 5) R_{amb} is the convection and/or radiation resistance between the compensation chamber wall and the surrounding. These various thermal resistances are usually deduced from the LHP geometry and the working fluid.

The mean temperatures of the compensation chamber and the evaporator metal masses, T_{R_m} and T_{E_m}, are deduced from the energy balances, given by Eqs. (4) and (5), respectively,

$$\frac{\partial T_{R_m}}{\partial t} = \frac{1}{\rho_m c_{p_m}\Omega_{R_m}}\left(\frac{T_{E_m} - T_{R_m}}{R_{\mathrm{ax}}} - \frac{T_{R_m} - T_R}{R_{\mathrm{conv}}} - \frac{T_{R_m} - T_{\mathrm{amb}}}{R_{\mathrm{amb}}}\right) \quad (4)$$

and

$$\frac{\partial T_{E_m}}{\partial t} = \frac{1}{\rho_m c_{p_m}\Omega_{E_m}}\left(\dot{Q} - \frac{T_{E_m} - T_v}{R_{\mathrm{vap}}} - \frac{T_{E_m} - T_{R_m}}{R_{\mathrm{ax}}}\right) \quad (5)$$

The evaporation mass flow rate at the porous wick surface $\dot{m}_v$, deduced from the evaporator heat distribution, is given by the Eq. (6):

$$\dot{m}_v = \frac{1}{\ell_{v_E} + c_{p_\ell}(T_v - T_R)}\left(\frac{T_{E_m} - T_v}{R_{\mathrm{vap}}} - \frac{T_v - T_R}{R_w}\right) \quad (6)$$

The heat leak $\dot{Q}_p$, which acts on the compensation chamber temperature variation [see Eq. (3)], is defined as the compensation chamber heat net balance with the evaporator and the ambient:

$$\dot{Q}_p = \left(\frac{T_v - T_R}{R_w}\right) + \left(\frac{T_{E_m} - T_{R_m}}{R_{\mathrm{ax}}}\right) - \left(\frac{T_{R_m} - T_{\mathrm{amb}}}{R_{\mathrm{amb}}}\right) \quad (7)$$

From the evaporator subsystem equations, it can be noticed that the evaporator global dynamic is governed by the thermal inertia of the evaporator and compensation chamber metal masses.

C. Condenser Subsystem

The condenser is usually divided into three regions: the superheated vapor flow, the two-phase flow, and the subcooled liquid flow. Assuming that the vapor line is perfectly insulated, the vapor temperature drop along the line can be neglected. Because the pressure continues to drop along the way, the vapor becomes more and more superheated relative to the local saturation pressure until it reaches the entrance of the condenser. As the total flow pressure drop should be lower than the maximum capillary pressure, the vapor superheat at the condenser inlet will never exceed a few Kelvins, particularly when ammonia is used as the working fluid. The vapor sensible heat usually corresponds to a few tenths of the heat load. Consequently, the length of the superheated vapor flow in the condenser is small compared to the length of the two other flow regions. Then, the length of the superheated vapor flow may be neglected, all the more because vapor desuperheating may appear at the end of the vapor line close to the condenser, due to the axial heat conduction through the vapor tube line. This approach justifies the

choice of the start point of the two-phase zone at the condenser inlet in the proposed model.

The condenser two-phase analysis, based on the system mean void fraction, has been first developed by Wedekind et al. [16]. The model of forced condensing flow for the two-phase region is formulated by means of the following assumptions: 1) the flow pattern is assumed to be invariant with time and annular type with a sharp decrease of the liquid/vapor interface, which implies that the mean void fraction $\bar{\alpha}$ is independent of time; 2) the viscous dissipation, the fluid compressibility effects, and the variation of the kinetic energy at the interface are neglected so that the two-phase zone can be considered to be in a uniform liquid–vapor saturation state T_C; 3) the capacitances of the fluid and the wall are neglected.

As a consequence, the two-phase region can be described by a homogeneous density $\rho_{2\varphi} = \rho_v\bar{\alpha} + \rho_\ell(1-\bar{\alpha})$ and a homogeneous enthalpy $H_{2\varphi} = \rho_v\bar{\alpha}h_v + \rho_\ell(1-\bar{\alpha})h_\ell$ independent of time (for a given local saturation temperature), and the conservation of mass in this region is given by Eq. (8):

$$A_C\rho_{2\varphi}\frac{\partial\bar{\eta}}{\partial t} = \dot{m}_v - \dot{m}_C^* \tag{8}$$

where $\bar{\eta}$ is the length of the two-phase region, and $\dot{m}_C^*$ is the instantaneous total mass flow rate of fluid leaving the two-phase region relative to the moving boundary of the two-phase region. This mass flow rate is coupled with the heat transfer through the heat sink and can be expressed using the energy conservation in the two-phase region, leading to Eq. (9):

$$A_C H_{2\varphi}\frac{\partial\bar{\eta}}{\partial t} = (\dot{m}_v - \dot{m}_C^*)h_v + \dot{m}_C^*\ell_{v_C} - \phi \tag{9}$$

where $\phi = h_C\pi D_C\bar{\eta}(T_C - T_{\text{rad}})$.

In Eq. (9), the first right-hand term is the advected enthalpy due to the vapor net accumulation, the second term is the condensation heat flux, and ϕ is the global heat transfer between the two-phase region and the heat sink, including heat transfer by transversal conduction and convection or radiation.

In the subcooled liquid region, the application of the conservation of mass and energy yields

$$-A_C\rho_\ell\frac{\partial\bar{\eta}}{\partial t} = \dot{m}_C^* - \dot{m}_\ell \tag{10}$$

$$-A_C\rho_\ell h_\ell\frac{\partial\bar{\eta}}{\partial t} = \dot{m}_C^* h_\ell(T_C) - \dot{m}_\ell h_\ell(T_{C,o}) - \phi_{C,\text{sub}} \tag{11}$$

where $\phi_{C,\text{sub}}$ is the global heat flux transmitted to the heat sink from the subcooled region.

The combination of Eqs. (8–10) yields after rearrangement the two-phase flow length, the condensate mass flow rate, and the saturation temperature:

$$\frac{\partial\bar{\eta}}{\partial t} = \frac{\dot{m}_v - \dot{m}_\ell}{A_C(\rho_{2\varphi} - \rho_\ell)} \tag{12}$$

$$\dot{m}_C^* = \dot{m}_v - \frac{\dot{m}_v - \dot{m}_\ell}{1 - \frac{\rho_\ell}{\rho_{2\varphi}}} \tag{13}$$

$$T_C = T_{\text{rad}} + \frac{\ell_{v_C}}{h_C\pi D_C\bar{\eta}}\left[\dot{m}_v - \frac{\dot{m}_v - \dot{m}_\ell}{1 - (\rho_\ell/\rho_v)}\right] \tag{14}$$

The boundary conditions of Eqs. (12–14) are the vapor and liquid mass flow rates, $\dot{m}_v$ and $\dot{m}_\ell$, respectively, and the radiator temperature T_{rad}. Considering the saturation state in the condenser two-phase flow region, the pressure p_C is deduced from T_C.

The analytical solution of Eq. (11) gives the temperature of the liquid at the condenser outlet, $T_{C,o}$, which depends on the two-phase flow length $\bar{\eta}$ compared to the total condenser length L_C:

$$T_{C,o} = T_{\text{rad}} + (T_C - T_{\text{rad}})\exp\left[-\frac{\pi D_C h_{\text{conv}}}{\dot{m}_\ell c_{p_\ell}}(L_C - \bar{\eta})\right] \quad \text{if } \bar{\eta} < L_C \tag{15}$$

and

$$T_{C,o} = T_C \quad \text{if } \bar{\eta} \geq L_C \tag{16}$$

It could be noticed that the viscous effects of the subcooled liquid flow in the condenser subsystem are added to the ones of the liquid flow in the liquid line [see the "liquid transport line" subsystem, Eq. (18)]. Neither liquid nor thermal inertia effects have been considered in the condenser subsystem so that the condenser global dynamic is then dominated by the coupling of the heat and mass transfer during the liquid charge or discharge of the condenser.

D. Liquid and Vapor Transport Lines

The liquid line subsystem is characterized by the liquid and the metal pipe, into which the liquid flows from the condenser to the compensation chamber. The liquid is assumed to be incompressible, which induces a constant mass flow rate along the liquid line. As the liquid temperature at the compensation chamber inlet $T_{R,i}$ has an important effect on the LHP operation temperature, it is necessary to follow the time variation of the liquid temperature T_L along the liquid line. The heat transfer process in the liquid subsystem involves thermal inertia of the liquid and the metal line, convection heat transfer between the liquid and the metal line, and convection or radiation heat transfer between the metal line and the ambient. As the Biot number is lower than one in the liquid line, the metal line acts like a thin metal layer. Then, the temperature variations of the metal line and the fluid are similar. The local temperature in the liquid line subsystem is formally given by the expression (17):

$$\frac{\partial}{\partial t}\int_0^{L_L} cT_L A_L\,\mathrm{d}l = \frac{\dot{m}_\ell}{\rho_\ell}cT_{C,o} - \frac{\dot{m}_\ell}{\rho_\ell}cT_R - \int_0^{L_L} h_{\text{amb}}\pi D_L(T_L - T_{\text{amb}})\,\mathrm{d}l \tag{17}$$

where $c = [\rho_m c_{p_m}(A_m/A_\ell) + \rho_\ell c_{p_\ell}]$ is the global thermal capacity of the liquid and the metal line.

The forces acting on the liquid play an important role on the liquid motion, particularly during fast transient changes, such as fast condenser liquid discharge during large heat load steps. The momentum balance equation, given by Eq. (18), has been established for the whole liquid volume constrained from the end of the condenser two-phase region to the liquid/vapor interface in the compensation chamber:

$$\frac{\mathrm{d}\dot{m}_\ell}{\mathrm{d}t} = \frac{1}{L_C - \bar{\eta} + L_L + (\Omega_{R_\ell}/2S_R)} \times \left\{-\frac{\dot{m}_\ell}{S_R}\frac{\mathrm{d}\Omega_{R_\ell}}{\mathrm{d}t} + \frac{\dot{m}_\ell^2}{\rho_\ell A_C} - \frac{\dot{m}_v^2}{\rho_\ell S_w} + p_C A_C - p_R A_L + \rho_\ell g A_L L_L\sin\theta - \frac{128}{\pi}\frac{(L_C - \bar{\eta} + L_L)}{D_L^4}\frac{\mu_\ell}{\rho_\ell}\dot{m}_\ell A_\ell\right\} \tag{18}$$

where L_L, L_C, and $\bar{\eta}$ are the lengths of the liquid line, the total condenser, and the condenser two-phase region, respectively. The liquid flow regime is considered laminar. The pressure p_C and the length $\bar{\eta}$ of the condenser two-phase region are calculated from the condenser model. The physical mechanisms in the liquid line, such as the liquid motion, as well as the thermal transfer along the liquid line, play an essential role on the LHP dynamic operation.

In the vapor line, the vapor flow is supposed to be incompressible (Mach < 0.01) and the metal line is adiabatic. Moreover, the evaporator groove pressure drops are supposed to be small compared to the vapor line pressure drop. Then, the groove vapor pressure is supposed to be homogeneous and close to the vapor pressure at the vapor inlet line. Neglecting the inertia effects in the vapor, the vapor pressure at the vapor line inlet p_v is deduced from Eq. (19):

$$p_v = p_C + \Delta p_V \tag{19}$$

where p_C is the condenser two-phase pressure and Δp_V is the viscous pressure drop along the vapor line. Δp_V depends on the vapor mass flow rate $\dot{m}_v$, which is calculated from Eq. (6), and depends on the nature of the vapor flow (laminar or turbulent).

III. Results

The present section is dedicated to the estimation of the model performance. This is first performed by comparison of the simulation results with the experimental measurements of Wrenn et al. [11] that are among the most extensive test available in the open literature including a detailed geometry and materials description of the loop components. In a second phase, we test the ability of the model to reproduce the low- and high-frequency temperature oscillations. As these oscillations are transient instabilities that are strictly induced by the coupling itself between the physics of the condenser, liquid line, and evaporator, the ability to reproduce these oscillating behaviors in amplitude and frequency provides a reliable estimation of the thermal-hydraulic coupling modeling choices.

A. Comparison with the Test of Wrenn et al.

Actually there are not many experimental studies available that present complete information on the thermal and hydrodynamic behaviors in the open literature. A detailed experimental transient test has been performed by Wrenn et al. [11] to study the LHP robustness. The comparison between these experimental results and those of the model allows one to validate the model in a transient test including heat load and sink temperature variations.

1. LHP Description and Transient Test

The LHP geometry characteristics, provided by Wrenn et al. [11], are summarized in Table 1. The LHP consists of an aluminum-extruded evaporator with a nickel wick of 1.5 μm pore radius, an inconel hydroaccumulator (reservoir), stainless steel transport lines, and an aluminum condenser. The reservoir/evaporator is designed to increase the evaporator conductance and to improve the heat exchange between the returning liquid and the fluid inside the reservoir/evaporator. The lengths of the condenser (condenser plus subcooler), the vapor and liquid lines, made of smooth tubing, are 6.36, 4.26, and 5.08 m, respectively. Ammonia is the LHP working fluid. The transient test was performed to simulate varying heat loads and condenser sink conditions. The heat load profile $\dot{Q}_{\text{load}}$ and the chiller temperature T_{rad} as a function of time are illustrated in Fig. 2. The condenser coolant temperature is held constant at 10°C for the first half of the test, and then changes to −20°C at a rate of 3.4°C/ min before returning to 10°C. The heater power at the evaporator ranges from 0 to 800 W.

Table 1 LHP geometry characteristics (Wrenn et al. [11])

Working fluid:	Ammonia
Evaporator:	Aluminum
	Active length: 330 mm
	Metal thermal mass: 2430 $\text{J} \cdot \text{K}^{-1}$
Primary wick:	Nickel
	Outer diameter: 19 mm
	Inner diameter: 9.9 mm
	Effective pore radius: 1.5 μm
	Porosity: 0.65
	Permeability: 0.75×10^{-13} m^2
	Effective thermal conductivity: 14.3 $\text{W} \cdot \text{m}^{-1} \cdot \text{K}^{-1}$
Bayonet:	Inner diameter: 4.93 mm
Reservoir:	Inconel
	Length: 114 mm
	Outer diameter: 79 mm
	Metal thermal mass: 1200 $\text{J} \cdot \text{K}^{-1}$
Condenser:	Aluminum
	Inner diameter: 3.81 mm
	Length: 5.94 m
Subcooler:	Aluminum
	Inner diameter : 3.81 mm
	Length: 419 mm
Vapor line:	Stainless steel
	Inner diameter: 4.57 mm
	Length: 4.26 m
Liquid line:	Stainless steel
	Inner diameter: 4.57 mm
	Length: 5.08 m

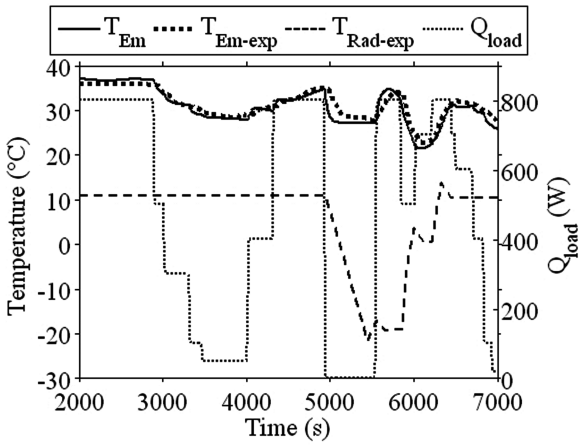

Fig. 2 Comparison of measured evaporator wall temperature to predicted temperature for the Wrenn transient test.

2. Model Results and Test Data Comparison

To compare the model and experimental results, the model constant parameters have to be calculated according to the experimental test setup. The heat load Q_{load} and the sink and ambient temperature, T_{rad} and T_{amb}, respectively, are clearly defined for the LHP test setup. The thermal masses in the evaporator and the reservoir, the axial conduction resistance between the evaporator and the compensation chamber metal body R_{ax}, and the overall thermal resistance through the porous wick R_w are calculated according to the LHP geometry, described by Wrenn et al. [11]. The convection resistance between the metal mass and the fluid of the compensation chamber is determined assuming liquid natural convection. R_{vap} is difficult to estimate (see evaporator submodel section), and there is a lack of information concerning the reservoir and the liquid line thermal insulation (h_{amb}) and concerning the heat transfer coefficient (h_C) in the heat sink. Consequently, these parameters are adjusted using the steady-state experimental values at $Q_{\text{load}} = 800$ W and $T_{\text{rad}} = 10$°C. R_{vap} and h_{amb} are adjusted to have a good accordance between the model results and the measurements for $(T_{Em} - T_R)$ and T_R, respectively. h_C is adjusted to have a complete condenser opening. The estimated parameters have been verified to correspond to physical values.

The plots of the temperatures at the evaporator saddle T_{E_m} and at the reservoir T_R, predicted by the model and measured, are compared in Figs. 2 and 3, respectively. The model correctly predicts trends in the data. Although the model seems to underpredict the measured temperature, the maximum difference between the predicted and measured temperatures does not exceed 2 K. One possible reason of the model underprediction at low heat flux may be caused by the overestimation of the heat transfer between the evaporator/reservoir and the ambient air fixed at 25°C.

The model assumption that the reservoir behaves as a uniform liquid–vapor saturation state seems to be in accordance with the evaporator/reservoir design, which tends to improve the heat exchange between the returning liquid and the fluid inside the reservoir/evaporator. The plot of the liquid temperature as the liquid enters the reservoir $T_{R,i}$ is shown in Fig. 4. With a liquid temperature variation up to 28 K, the maximum difference between the predicted and the measured liquid temperatures does not exceed 3.5 K.

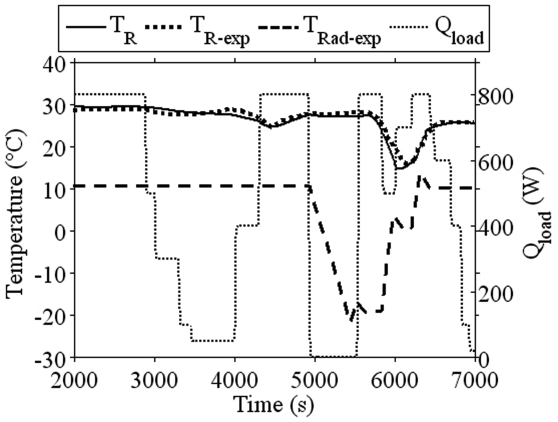

Fig. 3 Comparison of measured saturation temperature to predicted temperature for transient test.

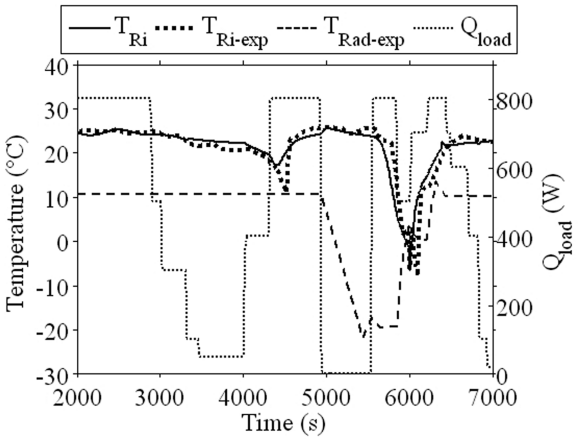

Fig. 4 Comparison of the measured liquid temperature at the reservoir inlet to the predicted temperature for the Wrenn transient test.

Although the model correctly predicts trends in the experimental data, a time lag of about 100 s can be observed between the predicted and measured temperatures, especially during large and abrupt heat load variations. The time lag is most evident at elapsed time around 4500 and 5500 s.

The plots of the two-phase flow length $\bar{\eta}$ and the pressure difference across the evaporator $(p_v - p_R)$ are shown in Figs. 5 and 6, respectively. As for the LHP thermal behavior, the LHP dynamic behavior is correctly predicted. The LHP operates in fixed conductance mode when the condenser length is fully used for condensation heat transfer. As observed in Fig. 5, the LHP operating

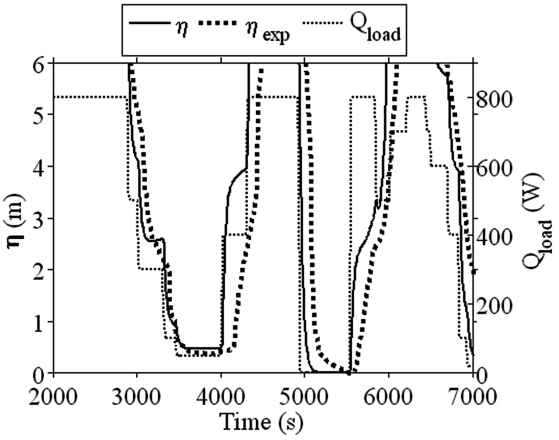

Fig. 5 Comparison of the measured condenser two-phase flow length to the predicted length for the Wrenn transient test.

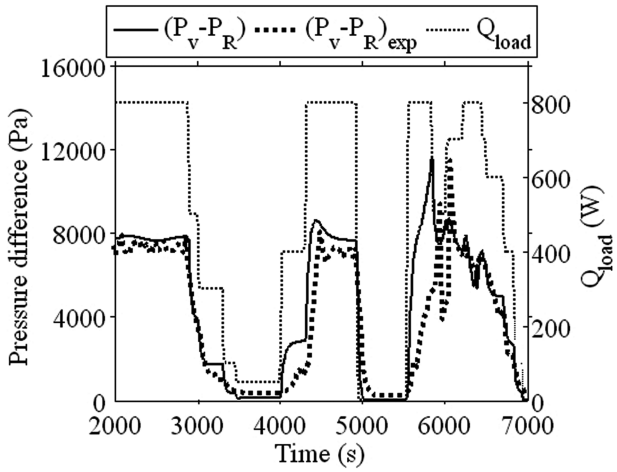

Fig. 6 Comparison of the pressure difference measured across the evaporator to the predicted pressure difference for the Wrenn transient test.

transition from variable to fixed conductance modes occurs at a heat load slightly lower than 800 W. As for the thermal behavior, the LHP dynamic response to a large and abrupt heat load variation is predicted with a time lag. The condenser liquid charge or discharge happens as soon as the heat load is stopped or applied. The choice not to consider thermal inertia into the condenser metal plate could explain this time lag on the condenser charge or discharge. However, an equivalent time lag was observed by Wrenn et al. [11], whose transient model takes into account the condenser thermal inertia. Then, this time lag can be due to an underestimation of the thermal inertia effect in the evaporator and reservoir walls. To simplify the most geometrically complex elements, the network of the evaporator/reservoir walls is just modeled by two nodes although the geometry of the evaporator is cylindrical and the heat source saddle is wide. Another way to explain this delay can be the overestimation of the heat leak between the evaporator grooves and the compensation chamber led by the assumption of a constant parasitic resistance. This parameter may actually depend on the phase distribution in the evaporator core specially at high heat loads.

B. Simulations of LHP Oscillating Behaviors

The following results indicate the ability of the transient model to simulate the LHP oscillations in frequency and amplitude. They have been obtained for the LHP geometry and characteristics described by Wrenn et al. [11]. Two different temperature fluctuation patterns have been highlighted, simply by modifying the LHP external conditions (heat load, sink temperature, ambient heat exchange with the liquid line).

1. High-Frequency Low-Amplitude Oscillations

The high-frequency low-amplitude oscillations are usually observed when the LHP operates in the fixed conductance mode. According to Ku [5], this type of oscillation is caused by the connection between the condenser and the reservoir which leads to a strong thermal-hydraulic coupling characterized by the unability of the vapor front to find a stable position at the condenser outlet. To simulate this pattern, two heat load levels have been imposed at the LHP evaporator, one varying from 20 to 800 W at time 1000 s, and the other varying from 800 to 450 W at time 4000 s. The sink and ambient temperatures are maintained constant with a temperature difference of 15 K. The variations of the temperatures, the two-phase flow length, and the liquid and vapor mass flow rates, obtained from the transient model, are shown in Figs. 7–9, respectively. An oscillating behavior is obtained for $\dot{Q}_{\text{load}}$ equal to 800 W, whereas the oscillations are absorbed for $\dot{Q}_{\text{load}}$ equal to 450 W. The oscillation frequency is equal to 1.8×10^{-3} Hz, and an oscillation phase shift mainly occurs in the liquid line. For $\dot{Q}_{\text{load}} = 800$ W, it could be

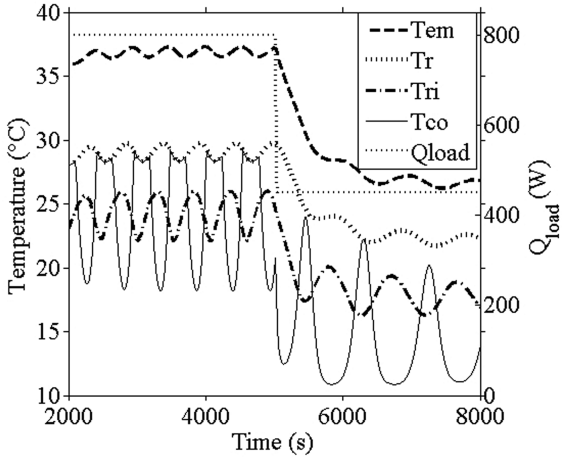

Fig. 7 Temperature oscillations for large heat loads.

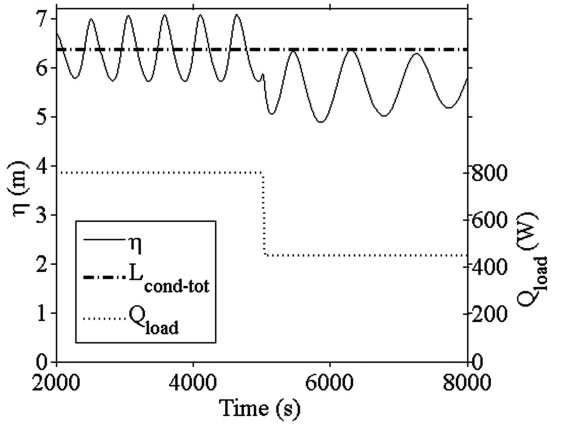

Fig. 8 Two-phase flow length oscillations for large heat loads.

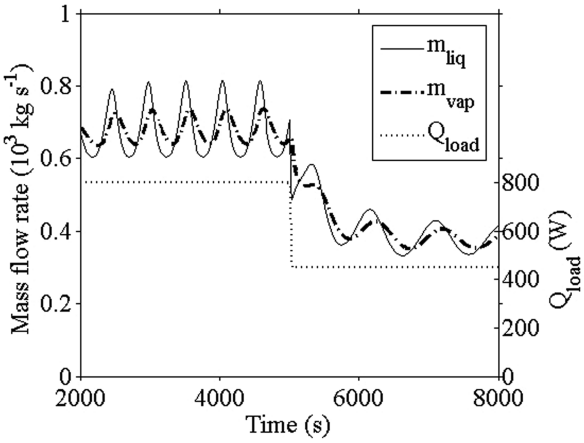

Fig. 9 Oscillations of liquid and vapor mass flow rates for large heat loads.

observed that the temperature oscillation amplitude is maximum at the condenser outlet $T_{C,o}$ ($\Delta T = 5$ K) and decreases as the liquid flows through the liquid line to the compensation chamber (Fig. 7). The temperature oscillation amplitude is minimum at the evaporator mass level (T_{E_m}) with a value of 0.8 K. The decrease of the temperature oscillation amplitude is caused by the heat transfer between the liquid line and the ambient and by the thermal inertia in the compensation chamber and evaporator masses. For $\dot{Q}_{\text{load}}=$ 800 W, the interface front in the condenser, described by $\bar{\eta}$, moves back and forth around the condenser outlet (6.36 m) with an amplitude of 0.5 m (Fig. 8). For $\dot{Q}_{\text{load}} = 450$ W, $\bar{\eta}$ is slightly lower than the total condenser length. The LHP operates at the limit between variable and fixed conductance modes, which explains why the oscillations are damped for $\dot{Q}_{\text{load}}$ lower than 450 W. As shown in Fig. 9, it could be noticed that the oscillation amplitudes of the mass flow rates are higher for the liquid flow ($\dot{m}_\ell$) than for the vapor flow ($\dot{m}_v$), and that these oscillations present a phase shift. The evaporator/compensation chamber mass can explain the large difference of the oscillation amplitude between the liquid and vapor mass flow rates.

The experimental results, presented by Kaya and Ku [4] whose LHP has similar characteristics to those of Wrenn et al., indicate an LHP oscillating behavior for a heat load of 500 W. With a temperature oscillation amplitude of 0.7 K at the evaporator and a frequency of 2.5×10^{-3} Hz, the oscillation characteristics of the experiment and of the transient model are in good accordance. For the experimental results, the oscillations appear for a lower heat load because of a shorter condenser total length ($L_C = 3$ m). From the experimental results presented by Chen et al. [7], the oscillation amplitude is maximal for a specific heat load, which depends on the LHP conditions, and their frequency increases with the heat load. An equivalent trend has been obtained from the transient model.

These results indicate that the modeling approach gives a good and quite accurate description of the dynamic couplings between condenser, liquid line, and the reservoir/evaporator.

2. *Low-Frequency High-Amplitude Oscillations*

The low-frequency high-amplitude oscillations are the result of the thermal and hydraulic couplings when the LHP operates in the region of variable conductance mode. According to Ku and Rodriguez [6], the mechanism that leads to a high-amplitude temperature oscillation is quite clear. The evaporator thermal mass modulates the net heat input into the evaporator by storing energy when the compensation chamber temperature is increasing and releasing energy when the compensation chamber temperature is decreasing. The change in the net evaporator heat load leads to the rise and fall of the compensation chamber temperature, which in turn amplifies the effect of heat load modulation by thermal mass. The net evaporator heat load will oscillate between a maximum value that is greater than the applied heat load $\dot{Q}_{\text{load}}$ and a minimum value that is smaller than $\dot{Q}_{\text{load}}$. The larger the variation of the net evaporator heat load, the larger the compensation chamber temperature oscillation.

To study this oscillatory behavior, a heat load of 25 W has been imposed to the LHP evaporator. The sink and ambient temperatures are maintained constant with a temperature difference of 35 K. The thermal masses attached to the evaporator are somewhat increased to a value corresponding to 10 kg of copper as in the experimental test performed by Ku and Rodriguez [6]. The startup simulation is achieved by controlling the value of the thermal resistance R_{vap} which is first maintained to a high initial value (corresponding to a small heat transfer coefficient between the liquid in the grooves/wick and the evaporator wall) until a defined wall superheat and then suddenly decreased to its default value. The variations of the temperatures, the two-phase flow length, and the liquid and vapor mass flow rates, obtained from the transient model, are shown in

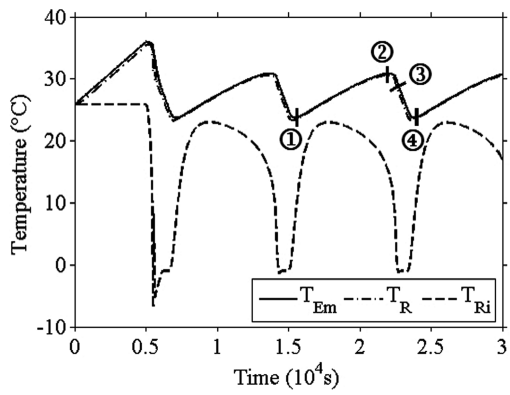

Fig. 10 Temperature oscillations for a low heat load ($Q_{\text{load}} = 25$ W).

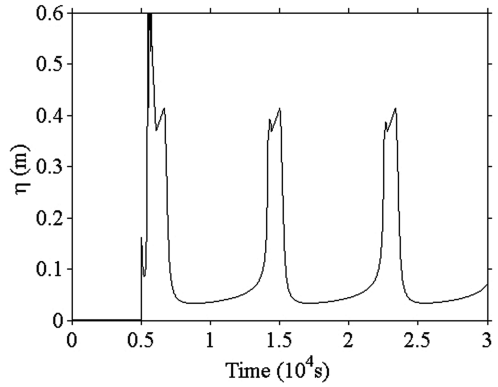

Fig. 11 Two-phase flow length oscillations for a low heat load (Q_{load} = 25 W).

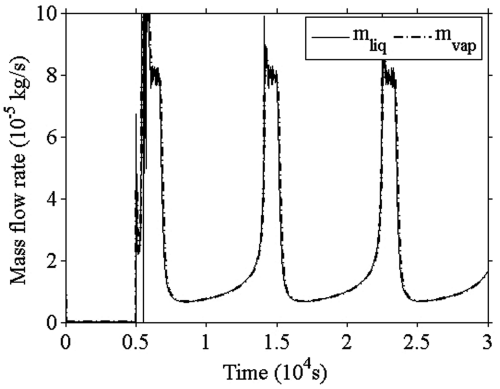

Fig. 12 Oscillations of liquid and vapor mass flow rates for a low heat load (Q_{load} = 25 W).

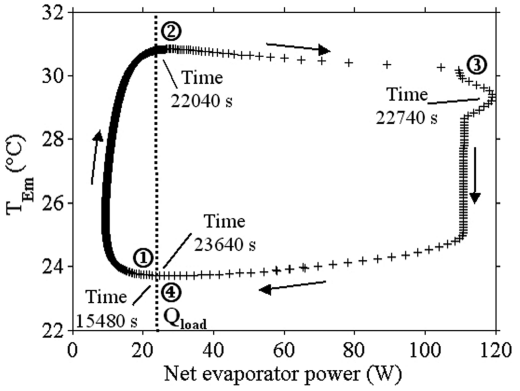

Fig. 13 LHP operating curve for an oscillating behavior in the variable conductance mode (Q_{load} = 25 W).

Figs. 10–12, respectively. After the LHP startup, the loop operates in an oscillating mode. The oscillation period is around 140 min, and the maximum temperature variation at the evaporator is equal to 8 K (Fig. 10). These oscillation characteristics are comparable to the ones of the experimental results (about 10 K in amplitude with a period of 120 min for the 25 W power test), which are performed in a quite similar loop device. This good accordance in amplitude and frequency between simulated and experimental tests shows again an appropriate modeling level for all the physical mechanisms involved in the reservoir as well as for its couplings 1) with the liquid line and 2) with the evaporator walls and wicks.

The transient LHP operating curve during one period of the low-frequency high-amplitude oscillation (points 1– 4 in Fig. 10) is shown in Fig. 13. The net evaporator heat load ($\dot{Q}_{net}$) corresponds to the heat flux at the evaporator inner wall, and the major part of $\dot{Q}_{net}$ goes into evaporation at the porous outer wick surface and is transferred to the condenser. The step between points 1 and 2, during which T_{Em} increases and $\dot{Q}_{net}$ is lower than $\dot{Q}_{load}$ (25 W), corresponds to the evaporator energy storage period. During this slow process (6560 s), part of the heat load is stored in the evaporator and reservoir metal masses, and $\dot{Q}_{net}$ reaches a minimum of 9 W. The step between points 2–4, during which T_{Em} decreases and $\dot{Q}_{net}$ is higher than $\dot{Q}_{load}$, corresponds to the evaporator energy release period. This step is a fast transient period (1600 s) as compared to the energy storage period, and $\dot{Q}_{net}$ reaches a maximum of 119 W (point 3). The step duration is correlated to the fluid hydrodynamic behavior (Figs. 11 and 12). These results agree well with the evaporator thermal mass modulation on the net heat load into the evaporator, which has been described by Ku and Rodriguez [6].

3. Remarks

It could be noticed that such oscillations have not been clearly observed from Wrenn et al.'s experimental results. The first reason is that the heat load step duration is of the same order or lower than the oscillation period, particularly for low heat fluxes. The second reason is that the temperature oscillation amplitude of the liquid at the reservoir inlet is reduced after flowing through the liquid line due to heat exchanges with the ambient environment. The measurement of the liquid temperature at the condenser outlet would be helpful to control the LHP oscillating behavior.

IV. Conclusions

In this study, a transient global model predicting the LHP dynamic behavior was presented in detail. The model of the whole loop has been divided into subsystems, for which transient mass, energy, or momentum conservation laws have been developed. This fundamentally based modeling approach proposes a description at the system scale as complete as possible but in the same time as explicit as possible. Then, this approach allows one to clear up and to analyze the complex linking of thermal-hydraulic mechanisms leading to the LHP transient behaviors.

The model validation consists first of the comparison of the calculation and experimental results for a transient test. With a liquid temperature global variation of 28 K, the maximum difference between the predicted and the measured temperatures along the LHP does not exceed 3.5 K. However a time lag still exists in high heat flux transitions. This may be due to the coarse model in the evaporator saddle or to the simplifying hypothesis of a constant purely conductive parasitic flux thermal resistance. Some efforts have then to be made in the modeling of the phase distribution in the evaporator core to improve the transient description of abrupt heat flux transitions.

On the other hand, two different temperature fluctuation patterns have been simulated: the "high-frequency low-amplitude" and the "low-frequency high-amplitude" temperature oscillations. Their characteristics (in frequency and amplitude) are of the same order as the ones observed during the LHP experimental tests available in the literature. That gives us the evidence that the modeling efforts are well adapted and the level of description appropriate for the oscillating behavior study. An extensive parameter sensitivities can now be performed to provide a more complete characterization of the oscillations.

Acknowledgements

The authors would like to thank K. Wrenn and S. Krein of Swales Aerospace, T. Hoang of TTH Research, and R. Allen of Motorola, for contributing test data from their internally funded test programs to aid in the development of the LHP transient model discussed in this paper.

References

[1] Ku, J., "Operation Characteristics of Loop Heat Pipes," SAE Paper 1999-01-2007, July 1999.

[2] Nikitkin, M., and Cullimore, B., "CPL and LHP Technologies: What

Are the Differences, What Are the Similarities," SAE Paper 981587, July 1998.
[3] Maydanik, Y. F., "Loop Heat Pipes," *Applied Thermal Engineering*, Vol. 25, April 2005, pp. 635–657.
[4] Kaya, T., and Ku, J., "Performance Characteristics of a Terrestrial Loop Heat Pipe," AIAA Paper 2000-0966, Jan. 2000.
[5] Ku, J., "High Frequency Low Amplitude Temperature Oscillations in Loop Heat Pipe Operation," SAE Paper 2003-01-2387, July 2003.
[6] Ku, J., and Rodriguez, J., "Low Frequency High Amplitude Temperature Oscillations in Loop Heat Pipe Operation," SAE Paper 2003-01-2386, July 2003.
[7] Chen, Y., Groll, M., Mertz, R., Maydanik, Y. F., and Vershinin, S. V., "Steady-State and Transient Performance of a Miniature Loop Heat Pipe," *International Journal of Thermal Sciences*, Vol. 45, Nov. 2006, pp. 1084–1090.
[8] Kaya, T., and Hoang, T., "Mathematical Modeling of Loop Heat Pipes and Experimental Validation," *Journal of Thermophysique and Heat Transfer*, Vol. 13, No. 3, 1999, pp. 314–320.
[9] Furukawa, M., "Model-Based Method of Theoretical Design Analysis of a Loop Heat Pipe," *Journal of Thermophysics and Heat Transfer*, Vol. 20, No. 1, 2006, pp. 111–121.
[10] Mena, F., Supper, W., and Puillet, C., "Design and Development of Loop Heat Pipe," SAE Paper 2000-01-2315, July 2000.
[11] Wrenn, K. R., Krein, S. J., Hoang, T. T., and Allen, R. D., "Verification of a Transient Loop Heat Pipe Model," SAE Paper 1999-01-2010, July 1999.
[12] Vlassov, V. V., and Riehl, R. R., "Modeling of a Loop Heat Pipe for Ground And Space Conditions," SAE Paper 2005-01-2935, July 2005.
[13] Zhao, T. S., and Liao, Q., "On Capillary-Driven Flow and Phase-Change Heat Transfer in a Porous Structure Heated by a Finned Surface: Measurements and Modelling," *International Journal of Heat and Mass Transfer*, Vol. 43, April 2000, pp. 1141–1155.
[14] Delil, A. A. M., Baturkin, V., Friedrikhson, Y., Khmelev, Y., and Zhuk, S., "Experimental Results on Heat Transfer Phenomena in Miniature Loop Heat Pipe with a Flat Evaporator," *Proceedings of the 12th International Heat Pipe Conference*, May 2002.
[15] Mishkinis, D., and Ochterbeck, J. M., "Conductive-Convective Effects in Determining Heat Leaks Across Loop Heat Pipe Wicks," *Proceedings of the 12th International Heat Pipe Conference*, May 2002.
[16] Wedekind, G. L., Bhatt, B. L., and Beck, B. T., "A System Mean Void Fraction Model for Predicting Various Transient Phenomena Associated with Two-Phase Evaporating and Condensing Flows," *International Journal of Multiphase Flow*, Vol. 4, March 1978, pp. 97–114.